MĂDĂLINA DUMITRIU [*]

INFLUENCE OF THE LONGITUDINAL AND LATERAL SUSPENSION DAMPING ON THE VIBRATION BEHAVIOUR IN THE RAILWAY VEHICLES

The paper focuses on the influence of the longitudinal and lateral suspension damping in correlation with the velocity upon the vibration behaviour of the railway vehicles while moving on a tangent track. The numerical simulations are developed based on a linear model of a 17-degree of freedom vehicle that allows the evaluation of the dynamic behaviour of the vehicle in a sub-critical velocity. Based on the response frequency functions of the vehicle in a harmonic and in a random behaviour, a series of basic properties of the stable behaviour of the forced lateral vibrations has been made evident, as well as the opportunities to lower the level of the carbody vibrations by changing the suspension damping.

1. Introduction

When a railway vehicle travels along a section of a tangent track, it vibrates laterally, due to the tangent track deviations and the reversed conicity of the wheels' lateral rolling surface. These vibrations, known under the name of hunting, intensify along with the speed increase, and when reaching a certain speed, called the critical hunting speed (V_{crt}), they become unstable [1]. The instability of the lateral vibrations in the vehicle manifests itself in large amplitude of the axles' transversal movement while consuming the track clearance, and extremely violent shocks affecting the riding safety and the comfort of the passengers.

The instability of the lateral vibrations limits the vehicle velocity, hence most studies are focused on this issue. Depending on the desired goal, there are used either simpler models with 4 or with 6 degrees of freedom in order to examine either the hunting of a bogie or of a 2-axle vehicle [2-7], or complex

[*] *Department of Railway Vehicles, University Politehnica of Bucharest, Bucharest, Romania; E-mail: madalinadumitriu@yahoo.com*

models considering the lateral movements of a 2-bogie vehicle [8-10] or even its movements in the vertical plan [11]. The issue of the stability in the vehicle lateral vibrations is particularly important during moving in high radius curves, as seen in the papers of Zboinski and Dusza [12, 13], Dukkipati and Swamy [14] or Lee and Cheng [11, 15]. These models have underlined various problems concerning the vehicle stability and the influence of some of its parameters upon the critical hunting speed. Many studies have examined the linear theory [16-18], but a better evaluation of the vehicle stability is derived when taking into account the non-linearities of the wheel-rail contact and the bifurcation theory [19-23].

The linear theory may be applied when the relative lateral wheel/rail displacements are enough small so that both geometry and tangential contact forces may be described using linear equations. This theory allows finding out the linear critical velocity based on the analysis of the sign of the real part of the roots of the characteristic equation.

When the non-linearities of the wheel-rail contact are considered in the model, the stability analysis points out that there is a non-linear critical velocity (beside the linear critical velocity), which is smaller than the linear one. It means that the lateral vibration of the vehicle can become unstable when its velocity is smaller than the value of the linear critical velocity. In terms of the bifurcation theory, the non-linear velocity is determined by the saddle-node bifurcation, while the linear velocity is determined by the subcritical Hopf bifurcation [12, 20]. However, in many applications, the difference between the two critical velocities is not big so that the vehicle is stable as long as its velocity is enough lower than the value of the linear critical velocity [24].

Nevertheless, the solving of the stability in the lateral vibrations does not provide an answer regarding the dynamic behaviour of the vehicle at the standard running speeds that are sub-critical. It should be mentioned that the behaviour of the vehicle in a sub-critical velocity is significant for its dynamic performance in terms of the running quality and comfort of the passengers.

To design a railway vehicle, it is important to know how various suspension parameters influence the dynamic behaviour in a sub-critical velocity. There are several open discussions on this issue. One of them concerns the influence of the longitudinal and lateral suspension damping upon the vibrations behaviour of the railway vehicles, which is exactly the topic of this paper. The starting point is that the relative displacements between the wheels and the rails are small in the sub-critical range of velocities and, hence, the influence of the contact non-linearities can be neglected and, consequently, a linear model is recommended for studying the lateral vibrations of the

vehicle. The influence of the velocity and of the longitudinal and lateral suspension damping on the carbody vibrations level is examined based on the frequency response functions of the vehicle in a harmonic and in a random condition. A series of basic characteristics of the stable behaviour in the forced vibrations in the horizontal plane is thus highlighted, as for instance the geometric filtering due to the vehicle wheelbase or the dependence on the dominant vibration modes of the vehicle on the velocity and on the random nature of the track lateral irregularities.

2. The mechanical model and the movement equations

The mechanical model for the study of the lateral vibrations in a railway vehicle, excited by the tangent track geometric deviations, is presented in Fig. 1 and 2. There will be considered the case of a 4-axle, 2-level suspension vehicle, which travels at a constant speed V on a tangent track, so that the behaviour of the lateral vibrations is stable ($V < V_{crt}$). It is about a model with 17 degrees of freedom that includes 7 bodies representing the carbody, the suspended masses of the bogies and the four wheelsets, connected among them via Kelvin-Voigt systems, by which the elastic and damping elements of the two suspension levels are modelled.

The vehicle carbody is assimilated to a 3-degree of freedom rigid body, with the movements of lateral displacement y_c, roll φ_c and yaw α_c. The following parameters of the carbody are of interest: wheelbase $2a_c$, mass m_c and the inertia moments around the longitudinal axis J_{xc} and the vertical axis J_{zc}. The height of the carbody centre of mass referred to the plan of the secondary suspension is h_c.

The bogie is also considered a 3-degree of freedom rigid body, namely lateral displacement y_{bi}, roll φ_{bi} and yaw α_{bi}, with $i = 1$ or 2. The main parameters of the bogies are the wheelbase $2a_b$, its mass m_b, the inertia moment referred to the longitudinal axis J_{xb} and the inertia moment referred to the vertical axis J_{zb}. The bogie centre of mass is at level h_{b1} to the primary suspension plane and at distance h_{b2} to the secondary suspension plane.

As for the wheelsets, they are considered able to do the following independent movements: a translation movement – the lateral $y_{oj,(j+1)}$, and a rotation movement – the yaw, $\alpha_{oj,(j+1)}$, where $j = 2i - 1$, with $i = 1$ or 2, while mentioning that the bogie i has the wheelsets j and $j+1$. The wheelsets parameters of mass m_o, and inertia moments J_{yo} and J_{zo} are taken into account.

The rigidities of the elastic elements of the secondary suspension are denoted with k_{xc}, k_{yc} and k_{zc}. To limit the yaw movement, each bogie is fitted with an anti-roll bar, whose rigidity is $k_{\varphi c}$. On the vertical direction,
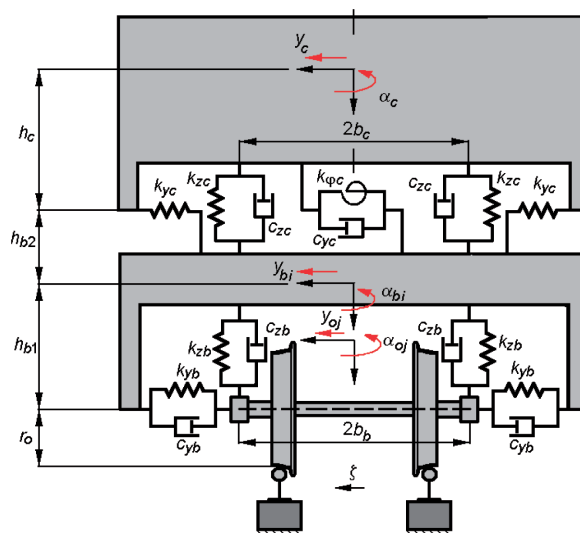
Fig. 1. The mechanical model of the vehicle for study of the lateral vibrations – front view
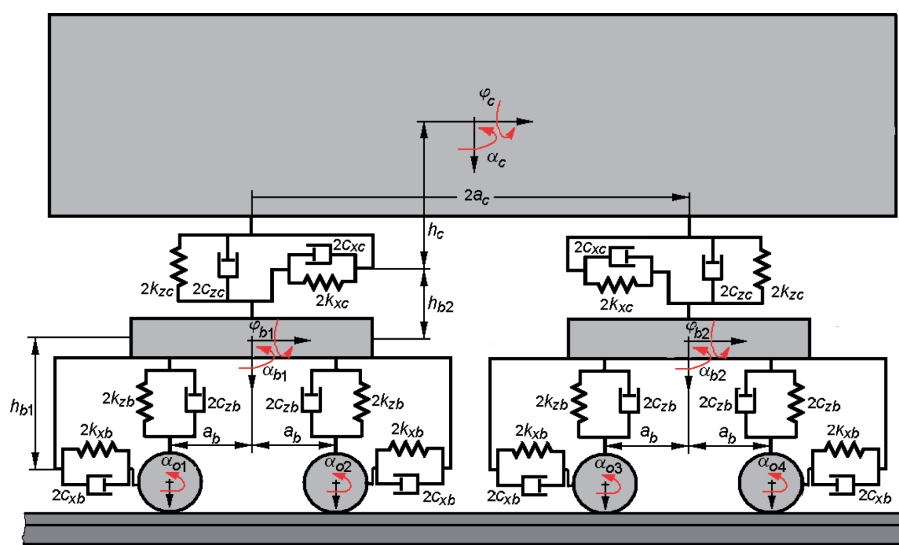

Fig. 2. The mechanical model of the vehicle for study of the lateral vibrations – side view

the secondary suspension of a bogie has two dampers, with the damping constant c_{zc} each, while on the lateral direction, it has one damper with a damping constant c_{yc}. The anti-yaw dampers, mounted on the lateral sides of the bogies, have the damping constant c_{xc}. The lateral base of the secondary suspension is noted with $2b_c$.

The primary suspension corresponding to a wheelset has the transversal base $2b_b$ and is modelled by three Kelvin-Voigt systems that operate on

translation in the longitudinal, transversal and vertical direction. These have the elastic constants k_{xb}, k_{yb}, k_{zb} and the damping constants c_{xb}, c_{yb} and c_{zb}.

The tangent track geometric with reference to the wheelsets j and $j+1$ are described by the functions $\zeta_{j,(j+1)}$, with $j = 2i - 1$, for $i = 1, 2$.

The equations of motion of the vehicle carbody (lateral, roll and yaw) are:

$$m_c \ddot{y}_c + c_{yc} \left[2(\dot{y}_c + h_c \dot{\varphi}_c) - (\dot{y}_{b1} + \dot{y}_{b2}) + h_{b2}(\dot{\varphi}_{b1} + \dot{\varphi}_{b2}) \right] + \\ + 2k_{yc} \left[2(y_c + h_c \varphi_c) - (y_{b1} + y_{b2}) + h_{b2}(\varphi_{b1} + \varphi_{b2}) \right] = 0. \tag{1}$$

$$J_{xc} \ddot{\varphi}_c + 2c_{zc} b_c^2 \left[2\dot{\varphi}_c - (\dot{\varphi}_{b1} + \dot{\varphi}_{b2}) \right] + \\ + c_{yc} h_c \left[2(\dot{y}_c + h_c \dot{\varphi}_c) - (\dot{y}_{b1} + \dot{y}_{b2}) + h_{b2}(\dot{\varphi}_{b1} + \dot{\varphi}_{b2}) \right] + \\ + (k_{\varphi c} + 2k_{zc} b_c^2) \left[2\varphi_c - (\varphi_{b1} + \varphi_{b2}) \right] + \\ + 2k_{yc} h_c \left[2(y_c + h_c \varphi_c) - (y_{b1} + y_{b2}) + h_{b2}(\varphi_{b1} + \varphi_{b2}) \right] - \\ - m_c g h_c \phi_c = 0 \tag{2}$$

$$J_{zc} \ddot{\alpha}_c + 2c_{xc} b_c^2 [2\dot{\alpha}_c - (\dot{\alpha}_{b1} + \dot{\alpha}_{b2})] + \\ + c_{yc} a_c \left[2a_c \dot{\alpha}_c - (\dot{y}_{b1} - \dot{y}_{b2}) + h_{b2}(\dot{\varphi}_{b1} - \dot{\varphi}_{b2}) \right] + \\ + 2k_{xc} b_c^2 [2\alpha_c - (\alpha_{b1} + \alpha_{b2})] + \\ + 2k_{yc} a_c \left[2a_c \alpha_c - (y_{b1} - y_{b2}) + h_{b2}(\varphi_{b1} - \varphi_{b2}) \right] = 0. \tag{3}$$

The equations of motion of lateral displacement, roll and yaw are given by the equations (3)–(5), for $i = 1, 2$ and $j = 2i - 1$:

$$m_b \ddot{y}_{bi} + c_{yc}(\dot{y}_{bi} - h_{b2}\dot{\varphi}_{bi} - \dot{y}_c - h_c \dot{\varphi}_c - (-1)^{i+1} a_c \dot{\alpha}_c) + \\ + 2c_{yb} \left[2(\dot{y}_{bi} + h_{b1}\dot{\varphi}_{bi}) - (\dot{y}_{oj} + \dot{y}_{o(j+1)}) \right] + \\ + 2k_{yc}(y_{bi} - h_{b2}\varphi_{bi} - y_c - h_c \varphi_c - (-1)^{i+1} a_c \alpha_c) + \\ + 2k_{yb} \left[2(y_{bi} + h_{b1}\varphi_{bi}) - (y_{oj} + y_{o(j+1)}) \right] = 0 \ ; \tag{4}$$

$$J_{xb} \ddot{\varphi}_{bi} + 2c_{zc} b_c^2 (\dot{\varphi}_{bi} - \dot{\varphi}_c) + c_{yc} h_{b2}(h_{b2}\dot{\varphi}_{bi} - \\ - \dot{y}_{bi} + \dot{y}_c + h_c \dot{\varphi}_c + (-1)^{i+1} a_c \dot{\alpha}_c) + \\ + 2c_{yb} h_{b1} \left[2(h_{b1}\dot{\varphi}_{bi} + \dot{y}_{bi}) - (\dot{y}_{oj} + \dot{y}_{o(j+1)}) \right] + \\ + 4c_{zb} b_b^2 \dot{\varphi}_{bi} + (k_{\varphi c} + 2k_{zc} b_c^2)(\varphi_{bi} - \varphi_c) + \\ 2k_{yc} h_{b2}(h_{b2}\varphi_{bi} - y_{bi} + y_c + h_c \varphi_c + (-1)^{i+1} a_c \alpha_c) + \\ + 2k_{yb} h_{b1} \left[2(h_{b1}\varphi_{bi} + y_{bi}) - (y_{oj} + y_{o(j+1)}) \right] + \\ + \left[4k_{zb} b_b^2 - g \left(h_{12} \frac{m_c}{2} + h_{b1} m_b \right) \right] \varphi_{bi} = 0, \tag{5}$$

where $h_{12} = h_{b1} + h_{b2}$;

$$J_{zb}\ddot{\alpha}_{bi} + 2c_{xc}b_c^2(\dot{\alpha}_{bi} - \dot{\alpha}_c) + 2c_{xb}b_b^2[2\dot{\alpha}_{bi} - (\dot{\alpha}_{oj} + \dot{\alpha}_{o(j+1)})]+$$
$$+2c_{yb}a_b[2a_b\dot{\alpha}_{bi} - (\dot{y}_{oj} - \dot{y}_{o(j+1)})] + 2k_{xc}b_c^2(\alpha_{bi} - \alpha_c)+ \qquad (6)$$
$$+2k_{xb}b_b^2[2\alpha_{bi} - (\alpha_{oj} + \alpha_{o(j+1)})] + 2k_{yb}a_b[2a_b\alpha_{bi} - (y_{oj} - y_{o(j+1)})] = 0.$$

For the wheelsets, the equations of motion of lateral displacement and yaw, with $i = 1, 2$ and $j = 2i - 1$, are:

$$m_o\ddot{y}_{oj,j+1} + 2c_{yb}\left[\dot{y}_{oj,j+1} - \dot{y}_{bi} - h_{b1}\dot{\varphi}_{bi} \mp a_b\dot{\alpha}_{bi}\right]+$$
$$+2k_{yb}\left[y_{oj,j+1} - y_{bi} - h_{b1}\varphi_{bi} \mp a_b\alpha_{bi}\right]+$$
$$+2\varphi\frac{\chi_y Q_o}{V}\dot{y}_{oj,j+1} + 2\frac{\chi_s r_o Q_o}{V}\dot{\alpha}_{oj,j+1}+ \qquad (7)$$
$$+2Q_o\varepsilon_s\frac{1 - \chi_s\varepsilon_o}{e_o}y_{oj,j+1} - 2\chi_y Q_o\alpha_{oj,j+1} =$$
$$= 2\lambda\frac{\chi_y Q_o}{V}\dot{\zeta}_{j,j+1} + 2Q_o\varepsilon_s\frac{1 - \chi_s\varepsilon_o}{e_o}\zeta_{j,j+1} \; ;$$

$$J_{zo}\ddot{\alpha}_{oj,j+1} + 2c_{xb}b_b^2(\dot{\alpha}_{oj,j+1} - \dot{\alpha}_{bi}) + 2k_{xb}b_b^2(\alpha_{oj,j+1} - \alpha_{bi}) + J_{yo}\frac{V}{r_o^2}\lambda\dot{y}_{oj,j+1}+$$
$$+2\chi_x Q_o\left(\frac{e_o\gamma_e}{r_o}y_{oj,j+1} + \frac{e_o^2}{V}\dot{\alpha}_{oj,j+1}\right) = J_{yo}\frac{V}{r_o^2}\lambda\dot{\zeta}_{j,j+1} + 2\chi_x Q_o\frac{e_o\gamma_e}{r_o}\zeta_{j,j+1} \; ,$$
$$(8)$$

where Q_o is the static load on the wheel, χ_x, χ_y and χ_s – creep coefficients, e_o, r_o – the coordinates of the wheel-rail contact points when the wheelset is in a median position on the track, γ_e – the effective conicity. Also, the following notations are used

$$\lambda = \frac{r_o\gamma_o}{e_o - r_o\gamma_o}, \quad \varphi = \frac{e_o}{e_o - r_o\gamma_o}, \quad \varepsilon_s = \frac{e_o}{\rho_w - \rho_r}\frac{e_o + \rho_w\gamma_o}{e_o - r_o\gamma_o}, \quad \varepsilon_o = \frac{e_o + \rho_r\gamma_o}{e_o + \rho_w\gamma_o},$$
$$(9)$$

with ρ_w and ρ_r the radii of the wheel-rail rolling profiles and γ_o – the contact angle in the median position of the wheelset on the track.

The creep coefficients are calculated by applying the Kalker's linear theory [16]

$$\chi_x = \frac{Gab}{N}C_{11}, \quad \chi_y = \frac{Gab}{N}C_{22}, \quad \chi_s = \frac{G(ab)^{1.5}}{r_o N}C_{23}, \qquad (10)$$

where a and b are the semi-axes of the contact ellipse, G – the transversal elastic modulus, $N \approx Q_o$ the normal force and C_{ij} – the Kalker's coefficients.

3. The steady-state harmonic vibration behaviour

The track geometric deviations are considered have in a harmonic shape, with the wavelength Λ and amplitude ζ_0. With the reference to each wheelset, the deviations are described by the functions below

$$\zeta_{1,2}(x) = \zeta_o \cos \frac{2\pi}{\Lambda}(x + a_c \pm a_b); \quad \zeta_{3,4}(x) = \zeta_o \cos \frac{2\pi}{\Lambda}(x - a_c \pm a_b), \quad (11)$$

where they are displaced, according to the vehicle wheelbases.

The functions $\zeta_{j,(j+1)}$, with $j = 2i - 1$ for $i = 1, 2$, can be expressed as time harmonic functions if considered that the position of the vehicle centre is given in the equation $x = Vt$. It results in

$$\zeta_{1,2}(x) = \zeta_o \cos \omega \left(t + \frac{a_c \pm a_b}{V} \right); \quad \zeta_{3,4}(x) = \zeta_o \cos \omega \left(t - \frac{a_c \mp a_b}{V} \right), \quad (12)$$

where $\omega = 2\pi V/\Lambda$ represents the angular frequency induced by the track excitation.

As for the vehicle response, it is assumed that this is also harmonic, with the same frequency as the track excitation. Under considered conditions, the coordinates describing the movements of the vehicle can be written in a general equation, as

$$p_k(t) = P_k \cos(\omega t + \varphi_k), \text{ with } k = 1 \div 17, \quad (13)$$

where P_k is the displacement amplitude and φ_k the phase of the coordinate k compared to the track deviation with respect to the vehicle centre; the vehicle model has 17 degree of freedom.

To solve the equations of the steady-state harmonic vibration behaviour, the complex quantities associated to the real ones will be adopted, as such:
– for the track deviations with the reference to the wheelsets

$$\bar{\zeta}_{1,2}(t) = \zeta_0 \cdot e^{i\omega \frac{a_c \pm a_b}{V}} \cdot e^{i\omega t} = \bar{\zeta}_{1,2} \cdot e^{i\omega t};$$

$$\bar{\zeta}_{3,4}(t) = \zeta_0 \cdot e^{-i\omega \frac{a_c \mp a_b}{V}} \cdot e^{i\omega t} = \bar{\zeta}_{3,4} \cdot e^{i\omega t}, \quad (14)$$

– for the coordinates of the vehicle movements

$$\bar{p}_k(t) = \bar{P}_k e^{i\omega t}, \quad (15)$$

where the complex amplitudes of the track deviation with the reference to the wheelsets are as below

$$\bar{\zeta}_{1,2} = \zeta_0 \cdot e^{i\omega \frac{a_c \pm a_b}{V}}; \quad \bar{\zeta}_{3,4} = \zeta_0 \cdot e^{-i\omega \frac{a_c \mp a_b}{V}} \quad (16)$$

and the complex amplitude of the coordinate k is

$$\bar{P}_k = P_k e^{i\varphi_k}, \tag{17}$$

where $i^2 = -1$.

Upon introducing the complex quantities (14-15) into the vehicle movement equations (1-8), a linear system of nonhomogeneous algebraic equations is obtained, with the complex amplitudes $\bar{P}_k$ of the vehicle movement coordinates being unknown, written under the matrix-like form

$$\mathbf{X}\bar{\mathbf{P}} = \bar{\mathbf{Y}}, \tag{18}$$

where $\bar{\mathbf{P}}$ is the vector of the complex amplitudes of the vehicle movement coordinates, $\mathbf{X}$ – the system matrix, and $\mathbf{Y}$ – the vector of the nonhomogeneous terms, of the excitation respectively.

Solving this system of equations allows one to determine of the vehicle frequency response factor. Thus, in some point P located in the carbody longitudinal symmetry plane, whose coordinates are x and h (see Fig. 3) in reference to the carbody centre of mass, the frequency response factor for the movement in a horizontal plane is calculated by the relation

$$\bar{H}_c(\omega, x, h) = \bar{H}_{y_c}(\omega) + x\bar{H}_{\alpha_c}(\omega) + h\bar{H}_{\varphi_c}(\omega). \tag{19}$$

where: $\bar{H}_{y_c}(\omega)$ – the frequency response factor for the lateral movement, $\bar{H}_{\varphi_c}(\omega)$ – the frequency response factor for the roll movement and $\bar{H}_{\alpha_c}(\omega)$ the frequency response factor for the yaw movement.
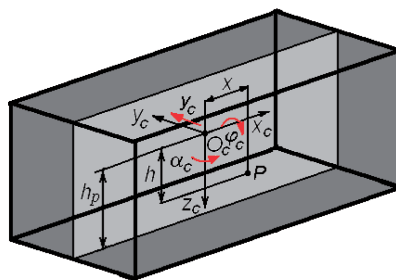

Fig. 3. The carbody longitudinal symmetry plane

Three reference points are defined – at the carbody centre and above the two bogies, located along the carbody longitudinal symmetry axis, at the floor level. To calculate the carbody response factors in these points, the following relations are used:

– for the response factor in the reference point at the carbody centre,

$$\bar{H}_{cm} = \bar{H}_c\left(\omega, 0, h_p\right) = \bar{H}_{y_c}(\omega) + h_p\bar{H}_{\varphi_c}(\omega); \tag{20}$$

– for the response factor in the reference points above the two bogies,

$$\bar{H}_{cb1,2} = \bar{H}_c(\omega, \pm a_c, h_p) = \bar{H}_{y_c}(\omega) \pm a_c \bar{H}_{\alpha_c}(\omega) + h_p \bar{H}_{\varphi_c}(\omega), \qquad (21)$$

where h_p is the distance from the carbody centre of mass to the floor level (see Fig. 3).

It is now possible to calculate the carbody acceleration response factor, based on the movement response factor. Thus, starting from relation (19), the response factor of the transversal acceleration in the point P can be obtained

$$\bar{H}_{ac}(x, h, \omega) = \omega^2 \bar{H}_c(x, h, \omega). \qquad (22)$$

While taking further the response factors defined in the equations (20) and (21) into account, the response factors for the transversal acceleration in the carbody reference points can be determined.

4. The behaviour of the random vibrations

The track deviations are considered to be random and stationary. Hence, the power density spectrum of the deviations can be approximated by means of a theoretical curve described in the equation [25]

$$S(\Omega) = \frac{A\Omega_c^2}{(\Omega^2 + \Omega_r^2)(\Omega^2 + \Omega_c^2)}, \qquad (23)$$

where Ω is the wavelength, $\Omega_c = 0.8246$ rad/m, $\Omega_r = 0.0206$ rad/m, and A is a constant that depends on the track quality. For a high quality track, $A = 2.119 \cdot 10^{-7}$ radm is adopted, while for a low quality track, the constant A will have the value of $6.124 \cdot 10^{-7}$ radm.

As a function of the angular frequency $\omega = V\Omega$, the power spectral density of the lateral deviations on the tangent track can be expressed as in the general equation

$$G(\omega) = \frac{S(\omega/V)}{V}. \qquad (24)$$

The relations (23) and (24) will give the power spectral density of the deviations in the form of

$$G(\omega) = \frac{A\Omega_c^2 V^3}{[\omega^2 + (V\Omega_c)^2][\omega^2 + (V\Omega_r)^2]}. \qquad (25)$$

Starting from the vehicle frequency response factor and from the track spectrum of the defects, one can calculate the power spectral density of the transversal movement of the carbody. Thus, for $\bar{H}_c(\omega, x, h)$ defined by relation (19) and $G(\omega)$ in the relation (25), the power spectral density of the

transversal movement of the carbody is obtained in the point P located in the longitudinal symmetry plan of the carbody

$$G_c(\omega, x, h) = G(\omega) \left| \bar{H}_c(\omega, x, h) \right|^2 . \tag{26}$$

As the response factor $\bar{H}_c(\omega, x, h)$ is replaced in equation (26) with the particular equations (20) or (21), the power spectral density of the carbody transversal movement can be calculated in the reference point at the carbody centre,

$$G_{cm} = G_c(\omega, 0, h_p) = G(\omega) \left| \bar{H}_{y_c}(\omega) + h_p \bar{H}_{\varphi_c}(\omega) \right|^2 \tag{27}$$

or in the reference points above the two bogies

$$G_{cb1,2} = G_c(\omega, \pm a_c, h_p) = G(\omega) \left| \bar{H}_{y_c}(\omega) \pm a_c \bar{H}_{\alpha_c}(\omega) + h_p \bar{H}_{\varphi_c}(\omega) \right|^2 ; \tag{28}$$

Further on, the power spectral density of the transversal acceleration can be calculated, and the following relation will be used

$$G_{ac}(\omega, x, h) = \omega^4 G_c(\omega, x, h) = \omega^4 G(\omega) \left| \bar{H}_c(\omega, x, h) \right|^2 . \tag{29}$$

This relation can be customized for any of the carbody reference points, if the power spectral density $G_c(\omega, x, h)$ is replaced with the expressions matching the reference points of the carbody (rel. (27-28)).

5. Numerical application

This section deals with the results of the numerical simulations concerning the vehicle frequency response in a steady-state harmonic and in a random vibration behaviour. Such simulations are based on the model and method described in the previous section. The reference values of the parameters in the vehicle model are used in the numerical simulations in Table 1. Table 2 features the geometric and kinematic parameters of the wheel-rail contact. The critical speed of the vehicle of 261.56 km/h [26] derives from the values in Table 1 and Table 2, but its maximum velocity is 200 km/h.

To analyse the influences of the suspension parameters upon the vehicle's vibrations behaviour, the damping ratio in the longitudinal and transversal directions of the two suspension levels will be introduced, as follows:

Table 1.

The reference parameters of the vehicle model

$m_c = 34000$ kg;	$2b_b = 2b_c = 2$ m
$m_b = 3200$ kg	$4c_{zc} = 68.88$ kNs/m
$m_o = 1650$ kg	$c_{yc} = 15.205$ kNs/m
$2a_c = 19$ m	$2c_{xc} = 50$ kNs/m
$2a_b = 2.56$ m	$4k_{zc} = 2.4$ MN/m
$J_{xc} = 57460$ kgm^2	$2k_{yc} = 340$ kN/m
$J_{zc} = 2456500$ kgm^2	$2k_{xc} = 340$ kN/m
$J_{xb} = 3200$ kgm^2	$4c_{zb} = 52.21$ kNs/m
$J_{zb} = 5000$ kgm^2	$2c_{yb} = 17.887$ kNs/m
$J_{zo} = 928.125$ kgm^2	$2c_{xb} = 50$ kNs/m
$h_c = 1.3$ m	$4k_{zb} = 4.4$ MN/m
$h_{b1} = 0.25$ m	$2k_{yb} = 5$ MN/m
$h_{b2} = 0.2$ m	$2k_{xb} = 70$ MN/m

Table 2.

The geometric and kinematic parameters of the wheel-rail contact

$\rho_w = 0.500$ m ; $\rho_r = 0.300$ m	$\chi_x = 205.716$
$r_o = 0.4598$ m ; $e_o = 0.754$ m ; $\gamma_o = 0.0495$	$\chi_y = 171.049$
$\gamma_e = 0.1237$	$\chi_s = 0.799$

– for the secondary suspension

$$\zeta_{xc} = \frac{4c_{xc}}{2\sqrt{4k_{xc}m_c}}\frac{b_c}{i_{zc}}; \quad \zeta_{yc} = \frac{2c_{yc}}{2\sqrt{4k_{yc}m_c}}; \quad (30)$$

– for the primary suspension

$$\zeta_{xb} = \frac{4c_{xb}}{2\sqrt{4k_{xb}m_b}}\frac{b_b}{i_{zb}}; \quad \zeta_{yb} = \frac{4c_{yb}}{2\sqrt{4k_{yb}m_b}}, \quad (31)$$

that have the following reference values $\zeta_{xc} = \zeta_{,yc} = 0.1$; $\zeta_{xb} = 0.07$; $\zeta_{yb} = 0.1$, in compliance with the model parameters in Table 1; i_{zc} and i_{zb} are the gyration radii of the carbody and bogie around vertical axe. The ranges of the damping ratio cover the intervals between 0.1 and 0.4 for ζ_{xc}, ζ_{yc} and ζ_{yb}, and, respectively, 0.07 and 0.4 for ζ_{xb}.

5.1. Verification of the model hypotheses

First of all, the hypotheses regarding the fact that the vehicle maximum velocity (200 km/h) takes a sub-critical value, and the hypothesis of model linearity have to be verified.

Figure 4 displays the linear critical velocity of the vehicle, which has been calculated using the sign of the real part of the roots of the characteristic equation, depending on the damping ratio of both primary and secondary suspension. On the one hand, the higher the damping ratio of the primary suspension, the lower the linear critical velocity. At the same time, the higher the damping ratio of the secondary suspension, the higher the linear critical velocity. Just in case, the lowest value of the linear critical velocity is 240.66 km/h which is higher than the maximum velocity of the vehicle and this corresponds to the following values of the damping ratio of the primary suspension: $\zeta_{xb} = 0.4$; $\zeta_{yb} = 0.4$.
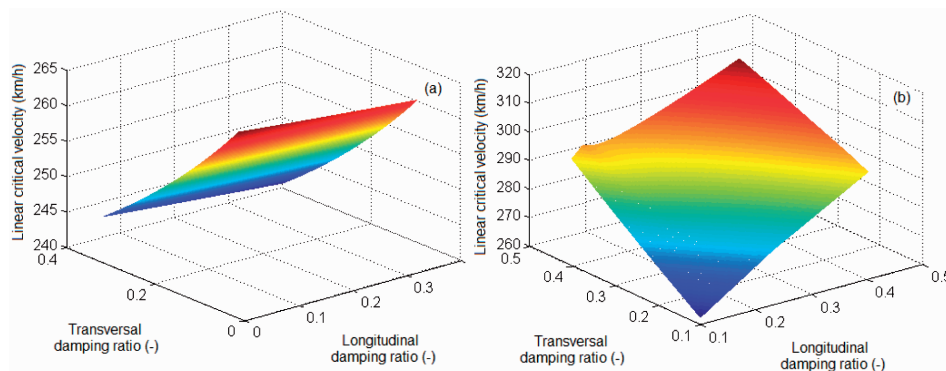
Fig. 4. Influence of the damping ratio on the linear critical velocity: (a) the damping ratio of the primary suspension; (b) the damping ratio of the secondary suspension

To verify the hypothesis regarding the linearity of the model, the vehicle ride at 200 km/h along a track with random lateral deviations is numerically simulated using the time-domain analysis method. The parameters values of the vehicle model correspond to the least favourable situation when the linear critical velocity is minimal, which means that $\zeta_{xb} = 0.4$; $\zeta_{yb} = 0.4$.

The track lateral deviation can be synthesized as a distance function from the power spectral density (eq. 23) using a method similar to that described in ref. [27]. Effectively, the track lateral deviation takes the shape of a sum of harmonic components with the wavelength between 3 and 229 m corresponding to the frequencies between 0.25 and 19 Hz.

The amplitudes of the harmonic components are extracted from the power spectral density and the phases have a uniform random distribution between $-\pi$ and π. Figure 5 presents the track lateral deviation which is obtained applying the method from above. The maximum amplitude of the lateral deviation is 5.02 mm and its effective value is 1.46 mm.
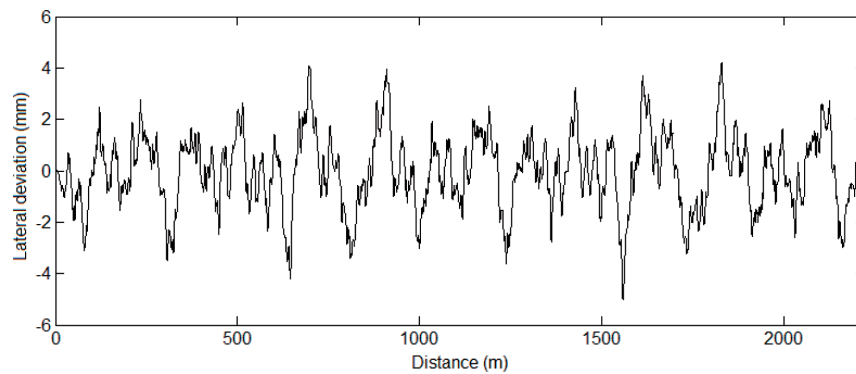

Fig. 5. Lateral deviation of the track

Figures 6 and 7 display the relative wheelset/track displacement and the creepage for all vehicle wheelsets and Table 3 presents the highest values and the effective value. The relative wheelset/track displacement takes the highest values for the leading wheelset of each bogie, and these values are smaller than 4.5 mm. For the new wheel/rail non-conformal profiles, such values allow us to adopt the linear model for the wheel/rail geometry.

Table 3.

Relative lateral wheelset/track displacement and the creepage

Wheelset	Relative lateral wheelset/track displacement		Creepage	
	Maximum value (mm)	Effective value (mm)	Maximum value (‰)	Effective value (‰)
#1 wheelset	4.25	1.27	1.97	0.37
#2 wheelset	2.96	0.90	1.69	0.31
#3 wheelset	4.33	1.29	1.50	0.27
#4 wheelset	3.02	0.91	1.34	0.24

On the other hand, the wheelsets of the first vehicle bogie exhibit the highest value of the creepage. However, these values are lower than 2‰ so that the hypothesis regarding the linearity of the creep forces is verified.
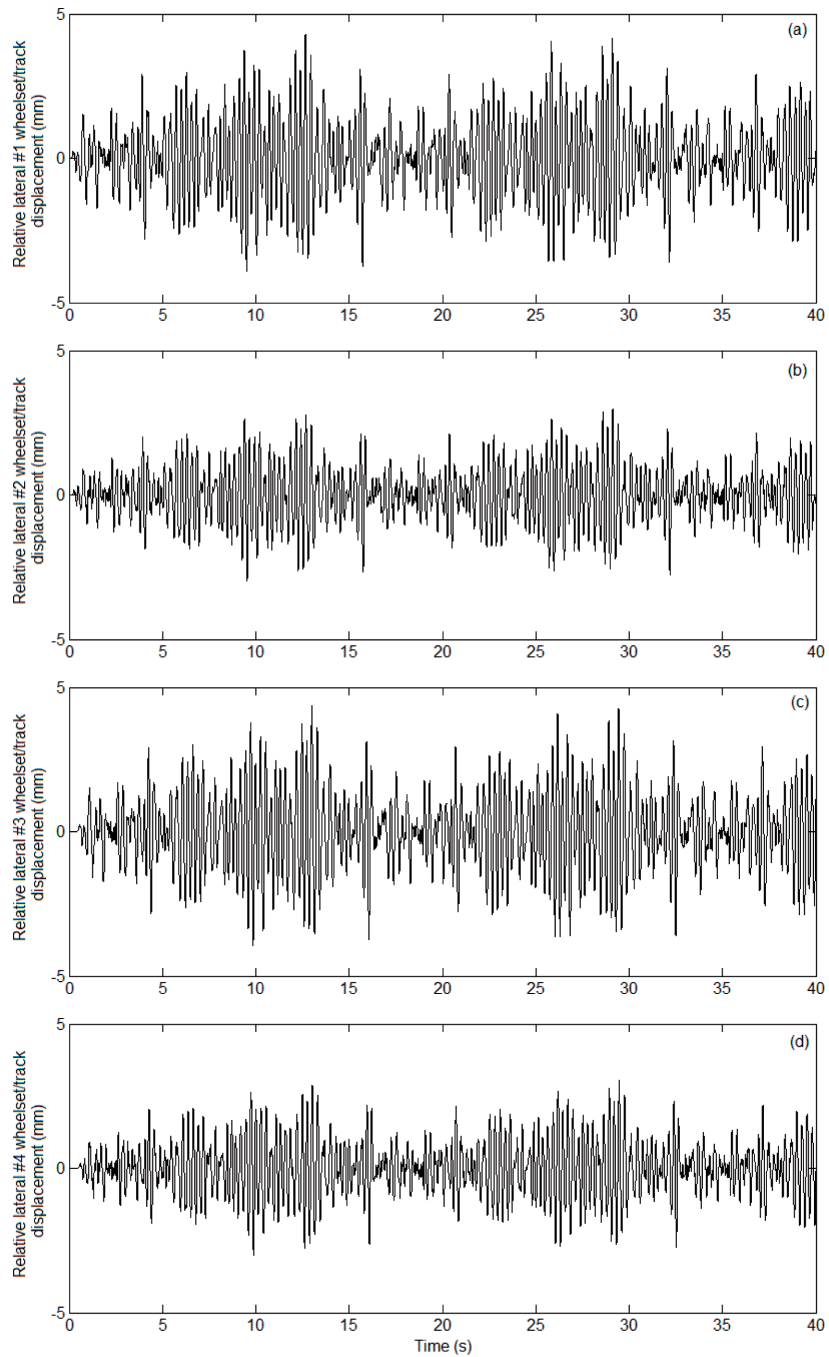
Fig. 6. Relative lateral wheelset/track displacement at 200 km/h: (a) for #1 wheelset; (b) for #2 wheelset; (c) for #3 wheelset; (4) for #4 wheelset
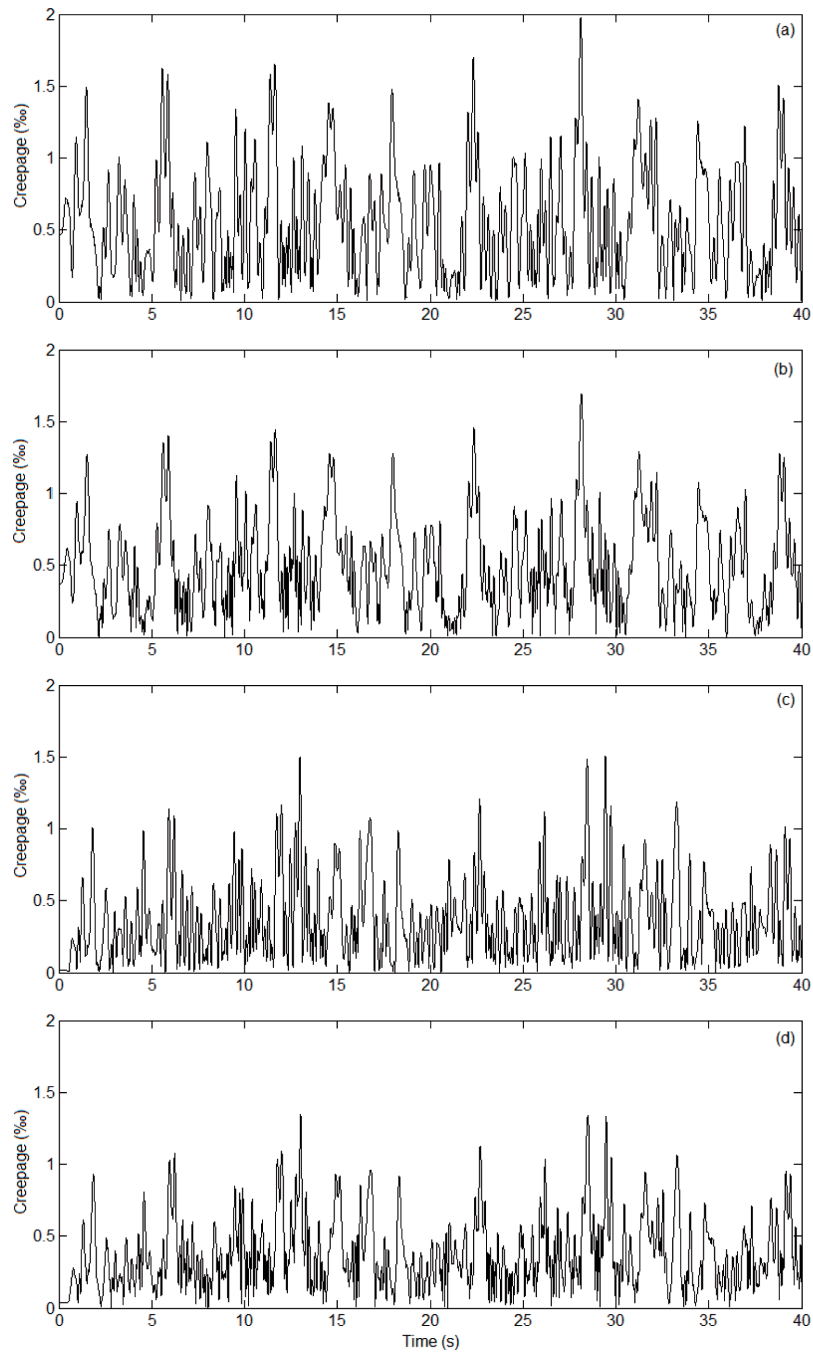
Fig. 7. Wheelset creepage: (a) for #1 wheelset; (b) for #2 wheelset; (c) for #3 wheelset; (d) for #4 wheelset

5.2. Influence of the longitudinal and lateral damping

In Fig. 8, the diagrams (a) – (c) show the response factor of the carbody movement in its reference points – at the centre and above the two bogies. The reference speeds of 100 km/h and 200 km/h are taken into account.
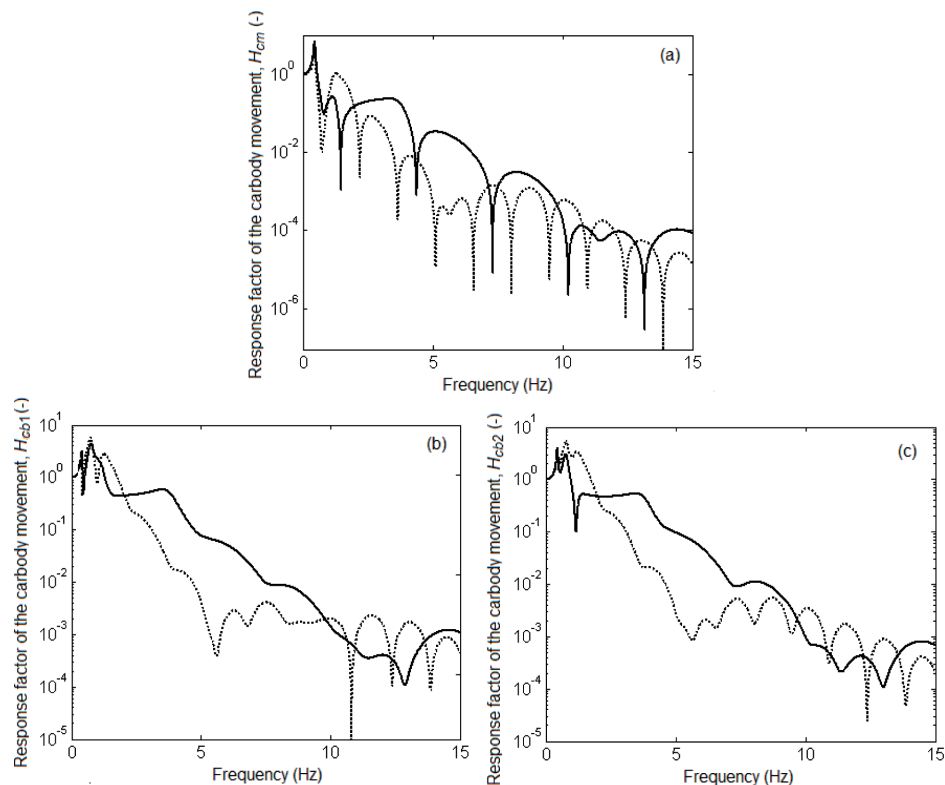
Fig. 8. Influence of the velocity on the carbody response factor: (a) at carbody centre; (b) above the front bogie; (c) above the rear bogie; $\cdots$, $V = 100$ km/h; ———, $V = 200$ km/h

Firstly, it should be mentioned that the carbody response at its centre comes from the coupled lateral displacement – the roll movement, and the diagram (a) shows the peaks of the resonance frequencies corresponding to this movement, which are 0.46 Hz and 1.21 Hz, respectively. Above the bogies, the carbody vibration comes from the coupled lateral displacement – the roll movement and also from the yaw movement. Thus, in the diagrams (b) and (c), another resonance peak is visible at 0.78 Hz, corresponding to the carbody yaw movement. Under considered conditions, the vibration level is usually lower at the carbody centre and increases against the two bogies. On the other hand, while examining the diagrams (b) and (c), we notice that the carbody response above the two bogies is not symmetrical, as there are

evident differences between the response factor calculated above the front bogie and the one above the rear bogie. This is an indication for a different vibration behaviour in these reference points, which is mainly due to the geometric filtering effect of the track deviations.

The geometric filtering effect is obvious in the diagrams (a) – (c) in the sense that the vehicle response includes a series of anti-resonance frequencies, along the peaks of the resonance frequencies. It is indisputable that the geometric filtering is more intense at the carbody centre, where the filtering effect given by the bogie wheelbase operates, and also by the carbody wheelbase. On the contrary, the filtering effect above the bogies is lower, as the geometric filtering here is only given by the bogie wheelbase in these points. Similarly, the geometric filtering is more efficient for low speeds, since it presents more filtering lobes and more anti-resonance frequencies, too.

As for the influence of the velocity on the carbody response to the track deviations, a general trend of magnification is visible in the level of vibrations along with the speed increase, valid for a large range of frequencies.

Instead, for low frequencies, where the resonance frequencies of the carbody movements are found, opposite effects can be seen. Thus, at the low resonance frequency of the lateral displacement – the roll movement, the carbody response amplifies with the velocity, whereas for the high frequency of lateral displacement – roll and the yaw frequency the carbody vibrations behaviour is lower at speed 200 km/h, compared to the one for speed 100 km/h. These opposite effects come from the geometric filtering, which shows a selective nature in dependence on the velocity.

The speed change leads to the displacement of the geometric filtering frequencies and of the anti-resonance frequencies in the diagram for the response factor. Should these frequencies come to reach the natural frequency of carbody vibration behaviour, then its influence would be much diminished. The velocities at which the geometric filtering frequencies coincide with the natural frequencies of the carbody movements can be obtained from the diagrams in Fig. 9 and Fig. 10. Figure 9 shows the response factor of the carbody movement in all three reference points at the resonance frequencies of the lateral displacement – roll coupled movement (0.46 Hz and 1.21 Hz) and in Fig. 10 we have the response factor of the carbody movement above the bogies at the resonance frequency of the yaw movement (0.78 Hz).

As pointed out earlier, the geometric filtering effect is noticed to have a selective nature, given by velocity, being more visible at low speeds of up to 50–60 km/h. While the velocity increases, the geometric filtering is more efficient at the high frequency of the lateral displacement – roll coupled movement than at the low frequency of the same movement or at the frequency of the yaw movement.
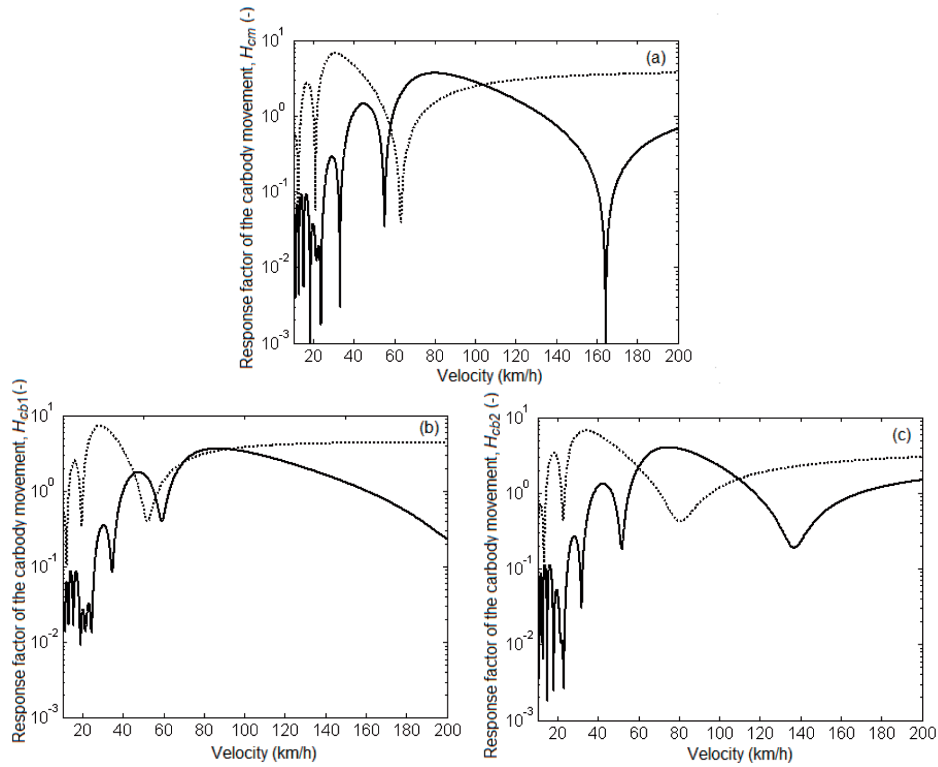
Fig. 9. The response factor of the carbody movement at the resonance frequencies of the lateral displacement – roll coupled movement: ——, 1.21 Hz, ····, 0.46 Hz; (a) at the carbody centre; (b) above the front bogie; (c) above the rear bogie
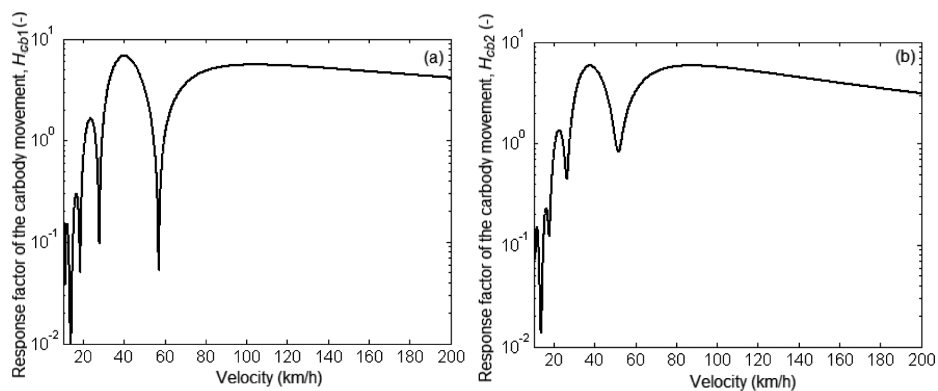

Fig. 10. The response factor of the carbody movement at the resonance frequency of the yaw movement (0.78 Hz): (a) above the front bogie; (b) above the rear bogie

The influence of the secondary suspension damping upon the carbody vibrations behaviour is then examined based on the diagrams in Fig. 11 which feature the response factor of the acceleration at the carbody centre

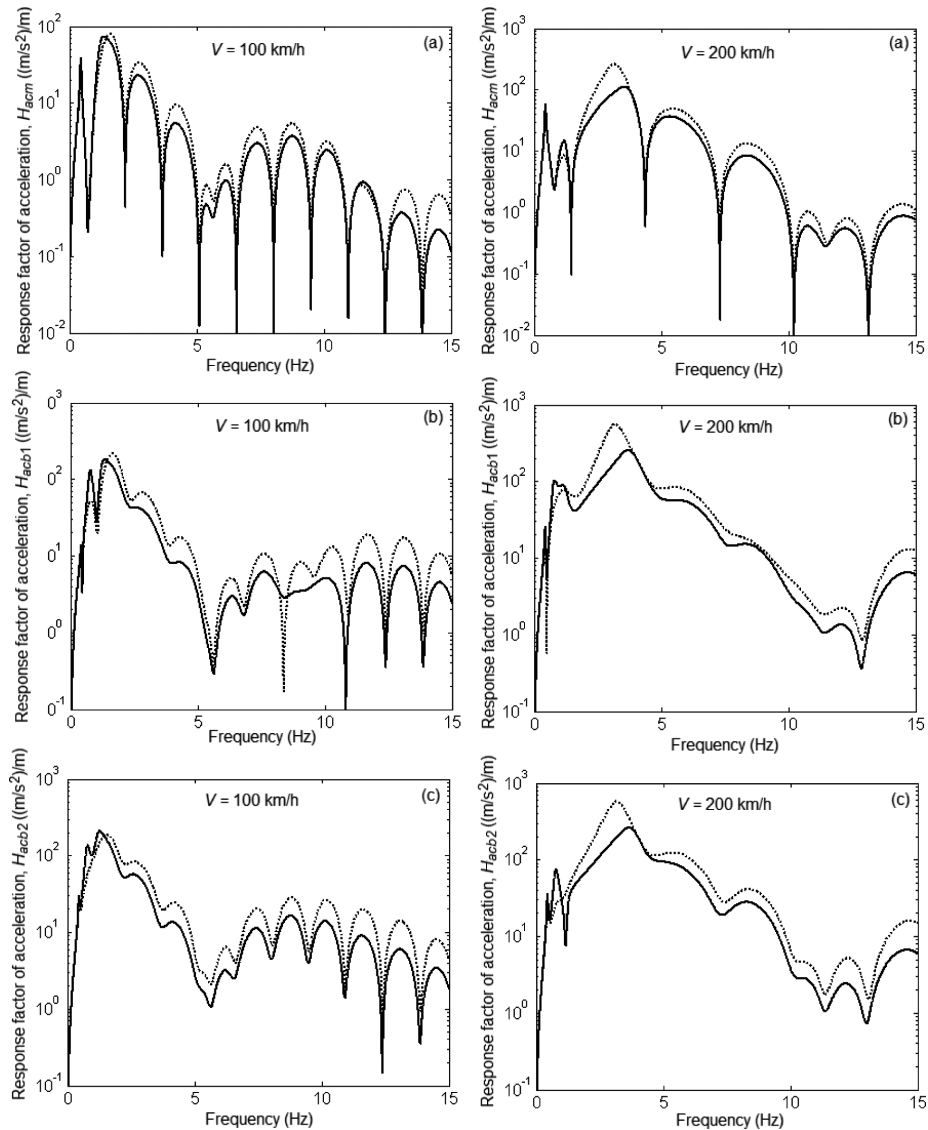and against the two bogies for the reference velocities of 100 km/h and 200 km/h.

Fig. 11. Influence of the secondary suspension damping on the response factor of the carbody acceleration: (a) at the centre; (b) above the front bogie; (c) above the rear bogie; ——, $\zeta_{xc} = 0.1$, $\zeta_{yc} = 0.1$; $\cdots\cdots$, $\zeta_{xc} = 0.3$, $\zeta_{yc} = 0.3$

As a rule, the increase of the damping in the secondary suspension leads to an amplification of the carbody vibrations. This observation is not valid for the domain of low frequencies, where the natural frequencies of the carbody movements are present.

One can very well notice the decrease of the response factor of the carbody acceleration above the bogies with the increase of damping, both for the resonance frequencies of the lateral displacement – the roll coupled movement and of the yaw movement. Such observations apply to both values of the reference velocity.

It is interesting to examine the influence that the secondary suspension damping on the longitudinal and transversal directions has on the carbody vibrations behaviour. To this purpose, the response factors of the acceleration to the resonance frequencies of the carbody movements in the three reference points have been calculated. Figure 12 shows the response factor of the acceleration at carbody centre, to the resonance frequencies of the lateral displacement – the roll coupled movement (0.46 Hz – diagram (a) and 1.21 Hz – diagram (b)), while Fig. 13 features the response factor of the acceleration above the two bogies to the resonance frequency of the yaw movement (0.78 Hz).
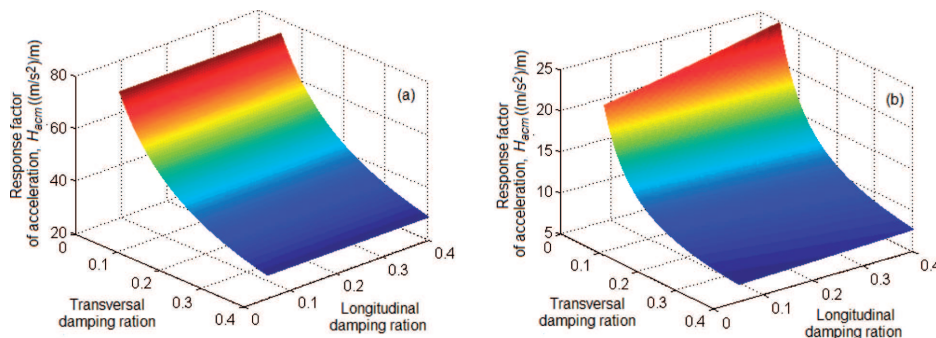

Fig. 12. Influence of the secondary suspension damping on the response factor of the acceleration at carbody centre: (a) low resonance frequency of the lateral displacement-roll coupled movement (0.46 Hz); (b) high resonance frequency of the lateral displacement-roll coupled movement (1.21 Hz)

The diagram (a) in Fig. 12 highlights the possibility of lowering the level in the carbody vibrations at the low frequency of the lateral displacement – the roll movement by increasing the damping ratio of the secondary suspension on the transversal direction. Similarly, a higher value of the damping can be noticed on the longitudinal direction that does not significantly influence the carbody response. On the contrary, for the high frequency of the lateral displacement-roll movement (diagram (b) – Fig. 12), the increase of ζ_{xc} leads to an amplification of the carbody vibrations behaviour. For instance, if ζ_{xc} increases from 0.1 to 0.4, the response factor of the carbody acceleration goes up by 2.21 (m/s^2)/m. While further examining the diagram (b), the response factor is smaller with the increase of the damping on the transversal direction. Thus, for the reference values of the damping on the transversal
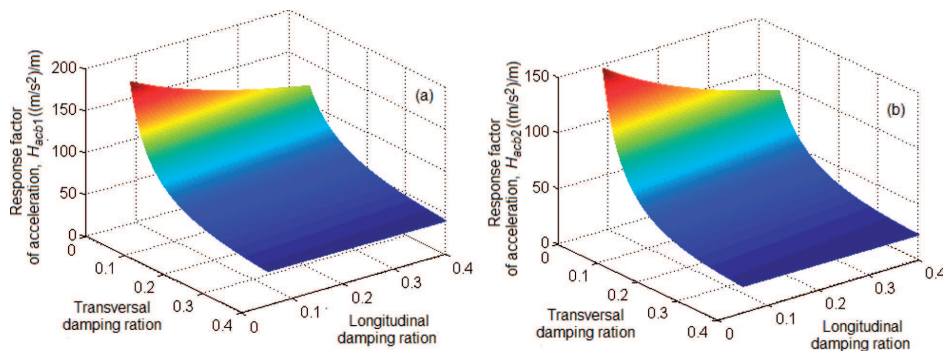
Fig. 13. Influence of the secondary suspension damping on the acceleration response factor above the bogies to the resonance frequency of the yaw movement (0.78 Hz): (a) above the front bogie; (b) above the rear bogie

and longitudinal directions (ζ_{xc} = 0.1, ζ_{yc} = 0.1), the response factor of the carbody acceleration is 14.33 (m/s^2)/m, and the increase of ζ_{yc} to 0.4 triggers a decrease of the response factor with 7.17 (m/s^2)/m.

For the resonance frequency of the carbody yaw movement (Fig. 13), a visible decrease in the response factor of the carbody acceleration is evident, by increasing the damping on the transversal direction. For example, while maintaining the reference value of damping on the longitudinal direction (ζ_{xc} = 0.1) and increasing the damping degree on the transversal direction from 0.1 to 0.4, the response factor lowers from 100.32 (m/s^2)/m to 40.27 (m/s^2)/m above the front bogie. A raise in the damping on the longitudinal direction leads to a lower vibrations behaviour in the carbody, which is more visible by lowering the response factor, especially when the transversal damping is low itself. Should ζ_{xc} rises four times, the response factor of the carbody acceleration above the rear bogie decreases with 17.65 (m/s^2)/m, when the reference value is maintained for ζ_{yc}.

The influence of the primary suspension damping on the carbody response in the three reference points is analyzed in Fig. 14. The increase in the primary suspension damping does not bring any evident changes in the vibrations level in the range of the carbody resonance frequencies. Lowering the level of carbody vibrations while the primary suspension damping raises is evident at frequencies higher than 4 Hz. For the speed of 200 km/h, one obtains high values of the damping ratio corresponding to the primary suspension amplify the carbody response against the yaw frequency of the axles (3.6 Hz).

The diagrams in Fig. 11 and Fig. 14 feature an important aspect, related to the resonance frequencies that dominate the spectrum of the response factor of the carbody acceleration. At the speed of 100 km/h, the dominant frequency is given by the high frequency of the lateral displacement – the
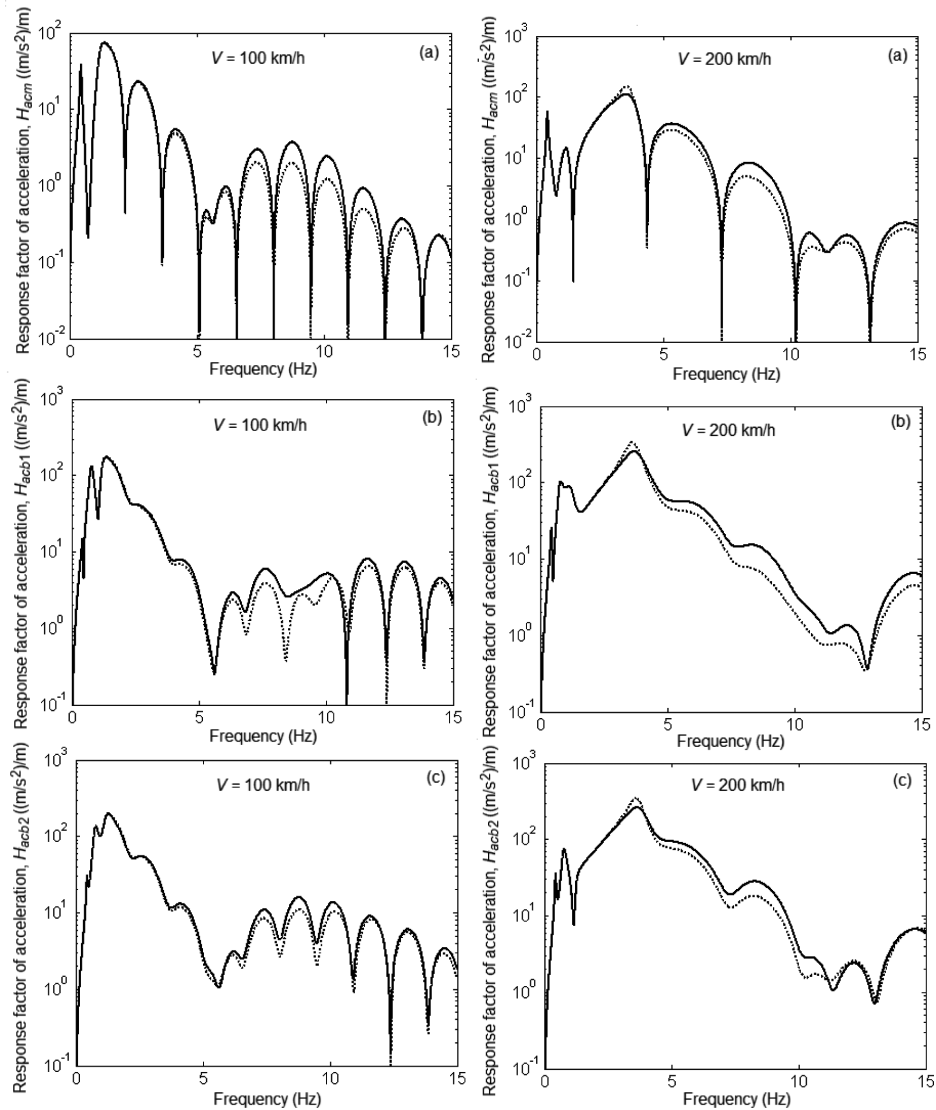
Fig. 14. Influence of primary suspension damping on the response factor of the carbody acceleration: (a) at the carbody centre; (b) above the front bogie; (c) above the rear bogie; —, $\zeta_{xb} = 0.07$, $\zeta_{yb} = 0.1$; $\cdots$, $\zeta_{xb} = 0.21$, $\zeta_{yb} = 0.3$

roll coupled movement. In the points above the two bogies, a significant contribution is also brought by the carbody yaw movement. Should the vehicle runs at speed of 200 km/h, the spectrum of the response factor of the carbody acceleration, in any of the reference points, is dominated by the resonance frequency of the yaw movement of the axles.

The track spectrum changes the ratio between the resonances, as shown below. To this end, the frequency response of the vehicle carbody to the
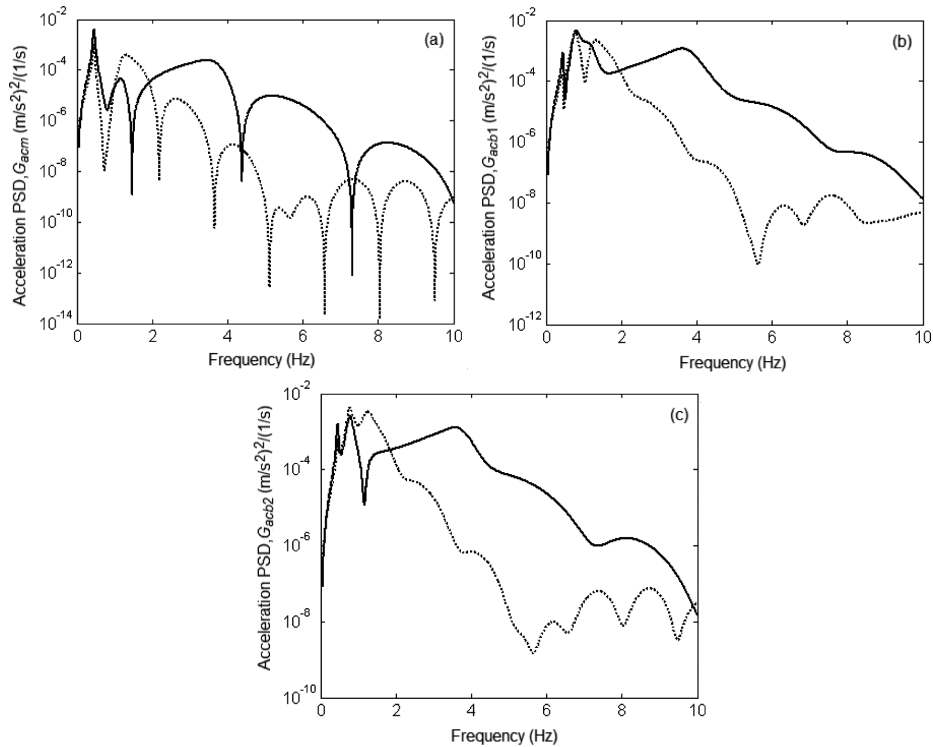
Fig. 15. Acceleration power spectral density: (a) carbody centre; (b) above the front bogie; (c) above the rear bogie; $\cdots$, $V = 100$ km/h —, $V = 200$ km/h

excitations represented by the random direction defects of the track will be examined.

The diagrams in fig 15 feature the spectra of the power density of the carbody acceleration at the centre and above the two bogies while moving on a high quality track ($A = 2.119 \cdot 10^{-7}$ radm) at the reference velocities of 100 and 200 km/h, respectively. One can notice that the frequency prevailing in the power density spectrum of the acceleration depends on the reference point being considered. At the carbody centre, what dominates is the low frequency of the lateral displacement – the roll coupled movement, while the frequency of the yaw movement and the high frequency of the lateral displacement – the roll movement are in control above the bogies.

One should be note the important influence of the yaw movement frequency of the axles at high velocities.

6. Conclusions

This paper is concerned with the behaviour of vibrations in the horizontal plane of a passenger vehicle while moving on a tangent track, with a sub-

critical velocity. Based on the response functions in a harmonic and in a random behaviour, we defined a number of characteristics specific to the vehicle's vibrations behaviour and the influence of the velocity on the level of vibrations in the carbody reference points – at centre and above the bogies.

Similarly, the influence of the damping of the two suspension levels on the carbody vibrations behaviour has been examined, and the possibilities to lower the level of vibrations to the vehicle's resonance frequencies have been highlighted.

The conclusion is that the frequency response at the carbody centre is dominated by the resonances of the lateral displacement – the roll coupled movement and influenced by the anti-resonances corresponding to the geometric filtering due to the wheelbases of the vehicle. Above the bogies, the frequency response is more intense, as the resonance of the yaw movement adds to the resonances of the lateral displacement – the roll coupled movement and also because the geometric filtering effect is reduced during filtering due to the bogie wheelbase. At higher velocities, close to the critical one, the resonance associated with the yaw movement of the wheelsets is present.

As for the geometric filtering effect due to the wheelbases of the vehicle, it has a selective nature depending on the running behaviour, being more evident at velocities of up to 50-60 km/h. Similarly, the geometric filtering is more efficient at the high frequency of the lateral displacement – roll coupled movement.

The frequency response of the carbody acceleration in the range of its resonances is diminished. Should higher values of the secondary suspension damping are adopted – the damping on the transversal direction is more efficient from this perspective. The primary suspension damping exerts no influence on the carbody response at low frequency, while high frequencies will trigger a certain decrease in the level of vibrations while damping increases.

While considering that the vehicle runs on a track with random deviations, we have mentioned that the carbody frequency response at its centre is dominated by the low frequency of the lateral displacement – the roll coupled movement, whereas the frequency of the yaw movement and the high frequency of the lateral displacement – roll movement prevail the power density acceleration spectrum above the two bogies. For high velocities, an important contribution can be attributed to the frequency of the yaw movement of the wheelsets.

REFERENCES

[1] Sebeşan I., Mazilu T.: Vibrations of the railway vehicles (in Romanian), MatrixRom Publishing House, Bucharest, 2010.

[2] Wickens A.H.: Static and dynamic instabilities of bogie railway vehicles with linkage steered wheelsets, Vehicle System Dynamics, Vol. 26, 1996, pp. 1-16.

[3] Whitman A.M.: On the lateral stability of a flexible truck, Journal of Dynamic Systems, Measurement and Control, Vol. 105, 1983, pp. 120-125.

[4] Whitman A.M., Molyneux J.E.: Limit cycle behavior of a flexible truck, Journal of Applied Mechanics, Vol. 54, 1987, pp. 930-934.

[5] Horak V., Wormley D.N.: Nonlinear stability and tracking of rail passenger trucks, Journal of Dynamic Systems, Measurement and Control, Vol. 104, 1982, pp. 256-263.

[6] Piotrowski J.: Stability of freight vehicles with the H-frame 2-axle cross-braced bogies. Simplified theory, Vehicle Systems Dynamics, Vol. 17, 1988, pp. 105-125.

[7] Haque I., Lieh J.: A study of parametric stability of railway vehicles, International Journal of Vehicle Design, Vol. 14, 1993, pp. 246-260.

[8] Park J.P., Koh H.I., Kim N.P.: Parametric study of lateral stability for a railway vehicle, Journal of Mechanical Science and Technology, Vol. 25, No. 7, 2011, pp. 1657-1666.

[9] Dikmen F., Bayraktar M., Guclu R.: Vibration analysis of 19 degrees of freedom rail vehicle, Scientific Research and Essays, Vol. 6, no. 26, 2011, pp. 5600-5608.

[10] Fan Y.T., Wu W.F.: Stability analysis of railway vehicles and its verification through field test data, Journal of the Chinese Institute of Engineers, Vol. 29, No. 3, 2006, pp. 493-505.

[11] Lee S.Y., Cheng Y.C.: Influences of the vertical and the roll motions of frames on the hunting stability of trucks moving on curved tracks, Journal of Sound and Vibration, Vol. 294, 2006, pp. 441-453.

[12] Zboinski K., Dusza M.: Self-exciting vibrations and Hopf s bifurcation in non-linear stability analysis of rail vehicles in a curved track, European Journal of Mechanics A/Solids Vol. 29, 2010, pp. 190-203.

[13] Zboinski K., Dusza M.: Bifurcation approach to the influence of lateral roll radius modelling and rail inclination on the stability of railway vehicles in a curved track, Vehicle System Dynamics Vol. 46, Supplement, 2008, pp. 1023-1037.

[14] Dukkipati R.V., Narayana S.: Lateral stability and steady state curving performance of unconventional rail trucks, Mechanism and Machine Theory, Vol. 36, 2001, pp. 577-587.

[15] Lee S.Y., Cheng Y.C.: Nonlinear analysis on the hunting stability of high-speed railway vehicle trucks on curved tracks, Transactions of the ASME Journal of Vibrations and Acoustics, Vol. 127 (4), 2005, pp. 324-332.

[16] Kalker J.J.: On the rolling contact of two elastic bodies in the presence of dry friction, Thesis, Delft, 1967.

[17] Knothe K., Böhm F.: History of stability of railway and road vehicles, Vehicle System Dynamics, 1999, Vol. 31, pp. 283-323.

[18] Wickens A.H.: Fundamentals of Rail Vehicle Dynamics – Guidance and Stability, Swets&Zertlinger, Netherlands, 2005.

[19] Polach O., Kaiser I.: On bifurcation analysis of complex railway vehicle models, ENOC 2011, 24-29 July 2011, Rome, Italy.

[20] Polach O., Kaiser I.: Comparison of methods analyzing bifurcation and hunting of complex rail vehicle models, Journal of Computational and Nonlinear Dynamics, Vol. 7, 2012, 041005 (8 pages).

[21] True H., Engsis-Karup A. P., Bigoni D.: On the numerical and computational aspects of non-smoothnesses that occur in railway vehicle dynamics, Mathematics and Computers in Simulation, Vol. 95, 2014, pp.78-97.

[22] Bigoni D., True H., Engsis-Karup A.P.: Sensivity analysis of the critical speed in railway vehicle dynamics, Vehicle System Dynamics, vol.52 Supplement 2014 pp. 272-286.

[23] Park J.P., Koh H.I., Kim N.P.: Parametric study of lateral stability for a railway vehicle, Journal of Mechanical Science and Technology, Vol. 25, No. 7, 2011, pp. 1657-1666.

[24] Polach O.: Comparability of the non-linear and linearized stability assessment during railway vehicle design, Vehicle System Dynamics, Vol. 44, Supplement, 2006, pp. 129-138.

[25] ORE B176. Bogies with steered or steering wheelsets, Report No. 1: Specifications and preliminary studies, Vol. 2, Specification for a bogie with improved curving characteristics, ORE, Utrecht 1989.

[26] Dumitriu M.: Influence of the suspension parameters upon the hunting movement stability of the railway vehicles, Mechanical Journal Fiability and Durability, issue 1, 2014, pp. 129-136.

[27] Dumitriu M.: Method to synthesize the track vertical irregularities, Scientific Bulletin of the Petru Maior University of Tîrgu Mureş, Vol. 11 no. 2, 2014, pp. 17-24.

Wpływ tłumienia wzdłużnego i poprzecznego w zawieszeniu na właściwości wibracji pojazdów szynowych

Streszczenie

W artykule skoncentrowano się na wpływie, jaki tłumienie wzdłużne i poprzeczne w zawieszeniu, w połączeniu z prędkością, ma na właściwości drgań pojazdów szynowych poruszających się po torze prostym. W oparciu o model pojazdu o 17 stopniach swobody opracowano symulacje numeryczne, które pozwalają na ewaluację właściwości dynamicznych pojazdu w zakresie prędkości podkrytycznych. Na podstawie funkcji odpowiedzi częstotliwościowych dla drgań harmonicznych i przypadkowych wyznaczono szereg podstawowych właściwości stabilnego zachowania się pojazdu w warunkach wymuszonych drgań poprzecznych. Pokazano też możliwości obniżenia poziomu drgań karoserii przez zmianę tłumienia w zawieszeniu.